Published in final edited form as:
Langmuir. 2009 July 7; 25(13): 7759–7765. doi:10.1021/la900332v.

Amplified Electrokinetic Response Concentration Polarization near Nanofluidic Channel

Sung Jae Kim[1], **Leon D. Li**[1,2], and **Jongyoon Han**[1,3,*]

[1]Department of Electrical Engineering and Computer Science, Massachusetts Institute of Technology, 77 Massachusetts Avenue, Cambridge, MA 02139, USA

[2]Harvard-MIT Division of Health Sciences and Technology, Massachusetts Institute of Technology, 77 Massachusetts Avenue, Cambridge, MA 02139, USA

[3]Department of Biological Engineering, Massachusetts Institute of Technology, 77 Massachusetts Avenue, Cambridge, MA 02139, USA

Abstract

Ion concentration polarization is the fundamental transport phenomenon that occurs near ion-selective membranes, but this important membrane phenomenon has been poorly understood due to theoretical and experimental challenges. Here, we report the first direct measurements of detailed flow and electric potential profiles within and near the depletion region. This work is an important step towards a full characterization of this coupled transport problem. Using microfabricated electrodes integrated with the microfluidic device, we measured and confirmed that the electric field inside an ion depletion region is amplified more than 30 fold compared to outside of the depletion zone due to the highly non-uniform ion concentration distribution along the microchannel. As a result, the electrokinetic motion of both fluid (electroosmosis) and particle (electrophoresis) was significantly amplified. The detailed flow profile within the depletion zone was also measured for the first time by optically tracking photobleached neutral dye molecules. We further showed that the amplified electrokinetic flows generated in this device may be used as a field-controlled, microfluidic fluid pump and switch.

1. INTRODUCTION

Recently, electrokinetic phenomena such as electroosmosis and electrophoresis have drawn significant attention as mechanisms for manipulating fluids and particles in micro/nanofluidic systems, with potential applications in the field of biology and chemistry [1,2]. Electrokinetic phenomena are the movements of fluids and particles driven by interfacial double layer charges induced by external forces such as an electric field or concentration gradient [3]. Among various forms of electrokinetic phenomena, electroosmotic flow (EOF) has been extensively studied since the very early stage of lab-on-a-chip devices. The velocity of fluid flow under EOF, $\mathbf{U}$, can be characterized by well-known Smoluchowski equation, $\mathbf{U}=-\varepsilon\zeta\mathbf{E}/\mu$, where ζ is the zeta potential of the charged wall and $\mathbf{E}$, ε and μ are the external electric field, permittivity and viscosity of fluid, respectively. With an equilibrium electrolyte concentration inside the electrical double layer (EDL), ζ is constant over the entire system and thus the velocity is linearly proportional to the local electric field.

*Correspondence should be addressed to Jongyoon Han: E-mail: E-mail: jyhan@mit.edu; phone: 617-253-2290; fax: 617-258-5846.

However, this equilibrium state is easily distorted when there is either a concentration gradient or non-uniform surface charge distribution.. These situations can be found in sample stacking [4,5] or microsystems with spatially heterogeneous surface properties [6–8]. Even more complex are cases where the structure of the Debye layer is directly manipulated via external forces [9–13]. Breaking the equilibrium condition inside the Debye layer through application of an external electric field gives rise to a non-uniform zeta potential which varies according to the Debye layer's ion concentration. This field induced, secondary EDL results in nonlinear electroosmotic slip near the micro and nanochannel interface. These complex non-equilibrium (or secondary) electrokinetic phenomena are scientifically rich and important in many engineering applications [14,15]. In particular, the development of novel micro/nanofluidic systems capable of actively changing the electrolyte concentration inside the electrical double layer have renewed the scientific interest in non-equilibrium EOF. Nanofluidic channels with critical dimensions of 10~100nm exhibit a unique perm-selectivity to ions due to effects from their overlapping electrical double layer [16–20]. A DC bias applied across such a nanochannel can initiate Ion Concentration Polarization (ICP) near the nanofluidic structures [21–24] by generating strong concentration gradients of ionic species through a perm-selective ion current. Once this concentration polarization is triggered, the concentrations of both cations and anions decrease on the anodic side of the junction (ion depletion) and increase on the cathodic side (ion enrichment). Good understanding of this phenomenon would be important in membrane applications including Nafion®-based electrolytes in fuel cells or biomolecule preconcentration systems [25]. Unfortunately, the scientific study of ICP has been limited since ICP is an interfacial phenomenon occurring at the nanomicro (or macro) junction, leading to experimental challenges inherent with multi-scale problems. In addition, all the transport parameters (flow, concentration, electric field) are coupled and must be solved concurrently for proper modeling [26].

In this paper, we present experimental results on ICP performed on microfabricated micro / nanofluidic devices. We find that due to the low ion concentration (low electrical conductivity) inside the ion depletion zone, the potential drop across the system becomes focused on the depletion zone. Also, any electrokinetic response (both electrophoresis and electroosmosis) in this region can be higher than normal due to higher effective zeta potential values caused by a non-uniform ion concentration. These two effects (high field and high effective zeta potential of walls and particles) combine to generate a unique, amplified electrokinetic response in and around the depletion zones. Previously, our group experimentally demonstrated that a circulating, vortex-like nonlinear electrokinetic flow characterized by faster speeds than that of equilibrium EOF can be induced near the perm-selective nanochannel along with the over-limiting current behavior [27]. However, tracking the flow profile within the strongly depleted zone has been difficult, since ICP phenomenon decreases the concentration of both negative and positive molecules. This practically prevents the use of standard flow tracking methods such as Particle Image Velocimetry (PIV), since most tracking particles are (moderately) charged in order to guarantee their stability in the solution. In addition, the electric field distribution arising from ICP is highly non-uniform and dynamically changing. Due to these combined effects of charge repulsions and non-uniformities of electric fields, the detailed study of nonlinear electrokinetic flow near nanojunctions under a strong ICP has not yet been achieved. In this paper, we measured, for the first time, the detailed electric field and flow profile within the depletion region and investigated the amplified electroosmotic and electrophoretic response within the ICP zone. The electric field distribution within the strongly depleted ICP region was measured by a microfabricated electrode array integrated with the microfluidic device. The detailed flow patterns within the depletion zone was determined by tracking the patterned photobleaching of neutral dye molecules combined with fluorescence imaging We find that the amplified EOF was strong enough to overcome and reverse the direction of pressure-driven flow, and may be used as a voltage controlled flow switching and

pumping device without requiring mechanical actuation. We identified two unique modes for amplified electroosmotic pumping, both of which can be useful for various applications.

2. EXPERIMENTAL METHODS

2.1 Device Fabrication

As shown in Figure 1a, the systems under study are composed of 2–3 parallel microchannels connected by nanochannels (or a nanoporous membrane). Compared to the classical membrane geometry that blocked a straight channel, fluid flow in our design is not blocked by the membrane but rather flows along it. We have fabricated the polydimethylsiloxane (PDMS) microfluidic chips with perm-selective nanojunctions using the previously published methods [28]. These devices are composed of a microchannel with either one (single gate (SG) device) or two (dual gate (DG) device) perm-selective nanojunctions for triggering ICP [27]. The SG device was favorable to acquire basic phenomenological effects while the DG device had an engineering advantage in obtaining fast and symmetric depletion boundaries. The microchannels used in both SG and DG device had the dimension of 15 μm depth and 100 μm height. For the particle tracking experiment, we fabricated the devices on both silicon and glass substrates using standard photolithography technique [29]. While the methods of fabrication were different in different measurements, the characteristic phenomena observed in these devices were all equivalent in all the devices used in this study.

Gold microelectrodes with titanium as an adhesion layer (25μm wide, 110nm height and 100 μm spacing between each electrode) for electric potential measurement were deposited on a glass substrate using standard evaporation/lift-off process (Ti: 10 nm and Au: 100 nm). The potential on each built-in electrode was measured using a Keithley 236 current-voltage source-measure unit (Keithley Instruments, Inc.), which has a high input impedance (200TΩ) minimize interference with the depletion and concentration processes.

2.2 Fluid and Particle Tracking Method

In order to track the flow through the depletion zone, a neutral dye (BODIPY 493/53, Invitrogen) was added to the main buffer solution, 1 mM phosphate (dibasic sodium phosphate) at pH = 8.7. To overcome the low solubility of the neutral dye, the dye was dissolved in an organic solvent such as methanol or ethanol first and then added to the buffer solution. Flow tracking was performed by photo-bleaching the dye through a 6 millisecond exposure to an Ar ion laser (Melles Griot, IEC 825-1:1993, 488nm, 100mW) beam. The laser beam was shaped into a line pattern using a cylindrical lens (ThorLABs, LJ18361L1-A) and 10X beam expander (ThorLABS, BE10M). Volumetric flow rate was measured by Nanoflow sensor (Upchurch, N-565) and the external pressure (both positive and negative) was generated by a syringe pump (Harvard apparatus, PHD 2200). 40 nm (Duke Scientific Corp.) carboxyl-terminated polystyrene beads were used for tracking amplified particle motions in the downstream desalting zone. All the flow patterns and particle motions were imaged with an inverted fluorescence microscope (Olympus, IX-51) and a CCD camera (SensiCam, Cooke corp.). Sequences of images were analyzed by Image Pro Plus5.0 (Media Cybernetics inc). A DC power supply (Stanford Research System, Inc.) was used to apply electrical potential to each reservoir through a homemade voltage divider. As shown in Figure 1a, Pt wires (Sigma Aldrich) were placed into each reservoir for proper electrical connections.

3. RESULTS AND DISCUSSIONS

3.1 Amplified Electric Fields with the depletion zone

In Figure 1b, the applied external electric field forms a normal electric field ($\mathbf{E_N}$) through the nanochannel. This initiates concentration polarization, where the ionic concentration in the

upper microchannel (anodic side) starts to become depleted and forms the ion depletion zone. This depletion zone spans the entire microchannel and limits the flow of charged molecules and particles. In effect, the depletion zone forms a barrier for charged molecules while allowing neutral molecules and water to pass through. The application of a tangential electric field ($\mathbf{E_T}$: V_H–V_L), where V_H and V_L are the applied electric potential at each reservoir, drives sample fluids including buffer ions and charged particles along $\mathbf{E_T}$ through the upper microchannel. As a result, ions, charged molecules and charged particles accumulate in front of the depletion zone and form the preconcentrated sample plug. At the same time, the downstream microchannel region (right hand side to the nanochannels) becomes largely desalted due to depletion, as any charged ions and molecules (both positively and negatively charged) are effectively blocked from passing the depletion zone.

The dynamically varying ion concentration in the microchannels greatly increases the challenges in analyzing the electric potential distribution inside the system. The electric potential distribution in this system could be highly focused and localized in the small but strongly depleted region and is dependent on the ion concentration changes near the depletion zone. To study the electric potential distribution *in situ*, we fabricate platinum electrode array as shown in the inset of Figure 2a. The electrodes are exposed to the main channel, allowing the electrical potential to be sampled at different points along the channel, including the depletion zone. The electric field both inside and outside the depletion zone was measured over the time period of depletion zone formation and expansion, as shown in Figure 2a. Although the external electric field of 30V/cm (50V-20V in 1cm long channel) was applied, $\mathbf{E}_{45}$ and $\mathbf{E}_{34}$ inside the depletion zone were measured to be ~1000V/cm and ~500V/cm. These field strengths are 33 fold and 17 fold higher respectively than expected values outside the depletion zone which has uniformly distributed ion concentrations. These measurements suggest that the depletion zone's averaged conductivity is in the order of ~0.1mS/m or less, a much lower value than the bulk conductivity value of 3.4mS/m (1mM Na_2HPO_4 buffer used). From Figure 2a, the potential drops between the electrodes at t=120s are $\Delta\varphi_{12}=\Delta\varphi_{23}=\sim 0.6$V, $\Delta\varphi_{34}=\sim 5$V, $\Delta\varphi_{45}=\sim 10$V and $\Delta\varphi_{56}=\sim -0.3$V. This should be the first, spatially-resolved, direct electric potential measurement within the depletion zone, which clearly confirms the existence of significant field amplification caused by strong concentration polarization (depletion) and an induced concentration gradient inside the depletion zone. Our findings agree with recent one-dimensional modeling studies [26, 30], which suggests that the electric field near the depletion zone can be amplified 20 times over than external field. $\mathbf{E}_{34}$ slowly increased because the depletion zone was expanding over the space between the two electrodes (e_3 and e_4) as a function of time, while $\mathbf{E}_{12}$ and $\mathbf{E}_{23}$ maintained their values because the depletion boundary did not reach e_3 within the 120 second experiment. $\mathbf{E}_{56}$ initially had positive values of E_x and soon decreased below 0, probably because the ion depletion zone initially grew between e_5 and the nanojunction (positive values of E_x). Then, the potential drop between the nanojunction and e_6 became more dominant over the gap between e_5 and e_6. This was caused by the different length of e_5-nanojunction and nanojunction-e_6. If the nanojunction and e_5 were exactly overlapped, $\mathbf{E}_{56}$ should have a negative value over the entire time span. Because of this effect, the measured values of $\mathbf{E}_{56}$ varied run to run compared with other traces, while quantitative trends were similar. We observed nearly a linear potential drop from the left-top reservoir (V_H) to the preconcentrated plug at the value of 30V/0.5cm=60V/cm (0.5cm is the length between reservoir and nanojunction), while a dramatic potential drop was seen inside the depletion zone below to V_L (denoted by V_N) due to the ground at the nanojunction as shown in schematics (Figure 2b). Namely, V_N is the electric potential at the nanojunction. More importantly, the electric field in the desalting zone has an opposite direction (negative value of E_{56} in Figure 2a) against the left hand side of microchannel. Under these electric fields conditions, the EOFs from both reservoirs pointed toward the nanojunctions (dotted blue arrow in Figure 2b), but with different magnitudes. The EOF of the left hand side is much stronger than that of the right hand side due to the amplified electric field inside the depletion zone,

resulting in an overall left to right fluid flow to maintain continuity (orange arrow in Figure 2b). These results are also confirmed by fluid motion tracking in Section 3.3 where a parabolic flow profile was observed as a result of an induced pressure field from the two different EOFs. This highly non-uniform electrical field and ion distribution also affects the electrophoresis of molecules and particles, which was also measured in the experiment.

3.2 Amplified Particle Motions

In order to track the electrophoretic particle motion within the depletion and downstream channel regions, we temporarily changed voltage configuration during device operation, which allowed the particles to move through the depletion zone, and then changed back to preconcentration voltage configuration in Figure 2c and 2d (See supplementary videos). We observed that, once the particles passed the depletion zone and entered the desalting zone, they travel at ~25 times faster than in the left hand side (buffer zones). The particle speed was 6μm/sec in the buffer zone and 140μm/sec in the desalted zone when V_H = 10V and V_L = 5V in the SG device (Figure 2c). In the DG device, the speeds were 20μm/sec in the buffer zone and 500μm/sec in the desalted zone when V_H = 20V and V_L =15V (Figure 2d). In the buffer zone and the concentrated plug zone, particles are mainly driven by the net flow (orange arrow in Figure 2b), with electrophoretic mobility pointing in the opposite direction (short red arrow in Figure 2b). In this case, negatively charged tracer particles were used. However, in the desalted zone, electrophoretic mobility (long red arrow in Figure 2b) is in the same direction as the net flow (orange arrow in Figure 2b), and the lower ion concentration is enhancing the effective zeta potential of the particle [31–33]. These two effects combine to explain the observed fast motion of the particles in the desalted zone.

3.3 Amplified Fluid Motions

To explore the electrokinetic flow inside and outside the depletion zone in detail, we visualized the flow patterns by tracking neutral dye molecules [34,35], while both positively and negatively charged species are generally inhibited from the depletion zone. Once the intense laser hit the fluorescent dye, the dye instantaneously loses its fluorescent signal and turns into black spots. Tracing the development of the photobleached region allows us to visualize the flow pattern. The extremely high electric field in the depletion zone caused faster EOF than any other zones (buffer, preconcentrating plug and desalted zone). This faster EOF pulled and pushed the fluid before and after the depletion zone, resulting in higher overall flow rate through the microchannel. Figure 3a shows the representative nonlinear electrokinetic flow pattern inside and outside the ion depletion region (See supplementary videos). The flow in the buffer zone upstream of the preconcentrated sample plug and in the desalted zone was similar to the typical plug type equilibrium EOF (U_{net}=~150μm/sec at V_H = 30V and V_L = 25V). However, the flow inside the ion depletion zone (between nanojunctions and preconcentrated plug) may be termed “boomerang type backflow.” In this flow configuration, a combination of high speed plug flow and parabolic type backflow needed to meet the continuity requirement created a unique flow profile (U_{circ}=~520μm/sec at V_H = 30V and V_L = 25V).U_{circ} was taken as the maximum velocity of the backflow in reverse direction (Thicker red arrow in Figure 3b). At the microchannel wall inside the depletion zone, the expected flow direction is along the amplified tangential field, $\mathbf{E_T}$. However, backflow was observed in the center of the microchannel since the low flow velocities outside the depletion zone retarded the total flow rate. Namely, there are circulating backflows inside the ion depletion zone and typical near-plug type flows in the desalted zone and buffer zone. Desalting mode was shown in the first schematic of Figure 3b, where the electrostatic repulsion inside the depletion zone was strong enough to completely block any charged species). Here, U_{net} is the actual flow coming out from the outlet reservoir, regardless of any complex local flow patterns which can be affected by locally changing driving forces such as zeta-potential and electric field strength. In order to obtain a much faster flow rate, we needed to increase $\mathbf{E_T}$ by (1) decreasing V_L or (2)

increasing V_H. In the first case, the preconcentrated sample plug moved closer to the nanochannel and the speed of plug flows increased. Further decreasing V_L induced much faster plug flow and finally the preconcentrated plugs flowed over the nanochannel. We name this condition burst mode, where the ion depletion zone can no longer span over the entire microchannel width. Here, the tangential flow through the microchannel overcomes the electrostatic repulsion inside the depletion zone. The velocity of circulating flow (U_{circ}) inside the depletion zone and plug flow (U_{net}) outside the depletion zone was simultaneously measured as shown in Figure 3c. The measurements were repeated five times for five different devices. The fitted red lines were used as a guide for the eye. At each line, V_H was fixed, while V_L was decreased to increase $\mathbf{E_T}$. The gray straight line represents the equilibrium EOF as a function of $\mathbf{E_T}$. Since the normal field (V_N to ground) through the nanojunction is mainly governed by the electrokinetic situation inside the depletion zone, especially U_{circ} (red lines), decreasing V_L led to decreasing U_{circ} ($\mathbf{E_N}$ dominating). On the contrary, U_{net} (black lines) increased along with $\mathbf{E_T}$ because it drove the fluid motion through the microchannel ($\mathbf{E_T}$ dominating). After bursting mode was reached, these two velocities merged. The velocity value of U_{circ} and U_{net} were much greater than that of equilibrium EOF's. A more detailed concentration and electrical field characterization would be needed in order to fully understand the flow mechanism in the burst mode. Still, these enhanced electrokinetic flows may be useful for fluid pumping and switching in general microfluidic systems. The transition point between burst and desalting modes is expected to be determined by the ion throughput of the nanojunction and the convection near the nanojunction. For the second case, V_H can be adjusted at higher value to increase the speed of plug flow, but the ion depletion boundary becomes unstable and fluctuates due to large $\mathbf{E_N}$ and destroys the preconcentrated plug [36].

3.4 Amplified Fluid Pumping

The amplified electrokinetic flow (AEK) described in the previous section has the capability to be used for microfluidic pumping and fluid control. The AEK flow can be turned on and off quickly using voltage manipulations as shown in Figure 4. The experiments were repeated at least 10 times using different devices so that we can guarantee reproducibility. The volumetric flow rates with AEK (~350nL/min) out of the microchip in this experiment were 5 times larger than that with equilibrium EOF (~70nL/min) in the DG device. We expect, however, that different designs of microchannel (changing length of downstream and upstream region) may enhance the maximum overall flow speed further, since the depletion region is generating the majority of the driving force for flow as seen from the flow profile (Figure 3b). The response time for flow pumping was less than 1 second, sufficiently fast for most microfluidic applications.

3.5 Amplified Fluid Switching

The AEK flow can be combined with external pressure-driven flow to make an efficient flow switching device, as shown in Figure 5. Initially, the flow was pumped solely by an external syringe pump as shown in the first photo (1) of Figure 5a. The net flow rate out of the center microchannel was electronically measured. In the figure, positive values indicate flow from the right reservoir to the left reservoir. In (2), the electric fields gradually increase to reach the threshold voltage while the external pressure was maintained. Eventually, the threshold to deplete the entire channel and initiate the AEK flow is reached, at which time the flow direction reverses as shown in Figure 5a (3) (See supplementary videos). The initial flow rate by syringe pump was +100nL/min which corresponds to 3.33mm/sec of linear velocity in the center microchannel. Above the threshold voltage, the ion depletion zone was established with $\mathbf{E_T}$ which had the reverse direction of the pressure field. From this moment, the net flow was immediately dropped to −100nL/min (+200nL/min in net flow rate) which is difficult to obtain with standard equilibrium EOF. Thus, the flow rate due to AEK flow can be at least 200nL/min from left to right. The fluid switching was tested several times in order to insure

repeatability. Theoretically, one can obtain this flow rate by equilibrium EOF with an electric field of O (10kV/cm). However, it is practically challenging to apply this extremely high voltage to the microchip due to an electrical breakdown and bubble generations. Figure 5b shows the immediate inversion of the flow rate when the threshold for AEK initiation is reached. The voltage at the left reservoir was increased at the rate of 1V/sec up to the threshold voltage. Then, it was decreased at the same rate. The threshold voltages for turning on and off the AEK pumping were different, showing hysteresis behavior. As demonstrated in our previous paper [27], the threshold behavior of ICP initiation is time-dependent. Even when electric potential values less than the threshold value are applied, the system can still initiate ICP, but perhaps with a longer time delay. When one increases the bias incrementally (from zero), then ICP can be initiated at lower potential values, compared with the case when potential is stepped up to the final value immediately. This is probably due to the sub-threshold permselective current during the voltage ramp-up, providing conditions more favorable for the generation of strong ICP even at lower voltages. Decreasing the voltage down from above the AEK threshold, however, destroys the depletion zone when the voltage drops to the threshold. This difference was observed as the hysteresis. We also observed that a greater threshold voltage is needed at higher buffer ionic concentration since more time is needed to achieve electrical double layer overlap [27]. However, the attainable flow rate was similar regardless of the ionic strength.

4. CONCLUSIONS

We have measured both the electric field and flow profile within the strongly depleted ICP regions near perm-selective nanojunctions and determined the exact flow mechanism in this coupled electrokinetic flow system. This study has several important implications in understanding the amplified electrokinetic response due to ICP. Once ion depletion is triggered, the electric field distribution in the system becomes highly non-uniform, generating extremely high electric fields within the ion depletion zone. As a result, electrokinetic responses are significantly amplified within that region and significantly affect the overall motion of both fluids and particles. Based on current results, efficient concentration of peptides and proteins previously reported [18] may be explained by AEK flow motions. Fast convection within the microchannel seems to prevent any significant development of space charge layer, as demonstrated by our concentration estimation within the depletion zone (via field measurement). However, the role of nonlinear electroosmotic slip [27,37], which is expected at the nanojunction interface, demands further investigation, possibly with higher spatial resolution in flow measurements. The AEK mechanism presented here is also an attractive candidate for microfluidic flow pumping and switching, as it can generate much higher flow rate at lower driving potentials than needed for equilibrium EOF and can be independent of the fluid's ion concentration. These systems can potentially replace pneumatic pumping actuation [38] with field-driven, high throughput microfludic pumping and switching, with wide applicability to the field of microfluidics.

Supplementary Material

Refer to Web version on PubMed Central for supplementary material.

ACKNOWLEDGEMENTS

This work was mainly supported by NIH (EB005743) and NSF (CBET-0347348).

REFERENCES

1. Beebe DJ, Mensing GA, Walker GM. Annu. Rev. Biomed. Eng 2002;4:261. [PubMed: 12117759]

2. Stone HA, Strook AD, Ajdari A. Annu. Rev. Fluid Mech 2004;36:381.
3. Hunter, RJ. Foundations of Colloid Science. Oxford University Press; 1989.
4. Jung B, Bharadwaj R, Santiago JG. Anal. Chem 2006;78:2319. [PubMed: 16579615]
5. Bharadwaj R, Santiago JG. J. Fluid Mech 2005;543:57.
6. Anderson JL, Idol WK. Chem. Eng. Commun 1985;38:93.
7. Stroock AD, Weck M, Chiu DT, Huck WT, Kenis PJ, Ismagilov RF, Whitesides GM. Phys. Rev. Lett 2000;84:3314. [PubMed: 11019078]
8. Ajdari A. Phys. Rev. Lett 1995;75:755. [PubMed: 10060106]
9. Schasfoort RBM, Schlautmann S, Hendrikse L, van den Berg A. Science 1999;286:942. [PubMed: 10542145]
10. Qian SZ, Bau HH. Anal. Chem 2002;74:3616. [PubMed: 12175145]
11. Moorthy J, Khoury C, Moore JS, Beebe DJ. Sensor Actuat. B-Chem 2001;75:223.
12. Urbanski JP, Thorsen T, Levitan JA, Bazant MZ. Appl. Phys. Lett 2006;89:143598.
13. Squires TM, Bazant MZ. J. Fluid Mech 2004;509:217.
14. Schoch RB, Han J, Renaud P. Rev. Mod. Phys 2008;80:839.
15. Prakash S, Piruska A, Gatimu EN, Bohn PW, Sweedlerx JV, Shannon MA. IEEE Sens J 2008;8:441.
16. Holtzel A, Tallarek U. J. Sep. Sci 2007;30:1398. [PubMed: 17623420]
17. Fu J, Schoch RB, Stevens AL, Tannenbaum SR, Han J. Nature Nanotech 2007;2:121.
18. Wang YC, Stevens AL, Han J. Anal. Chem 2005;77:4293. [PubMed: 16013838]
19. Chen GF, Tallarek U. Langmuir 2003;19:10901.
20. Huang KD, Yang RJ. Electrophoresis 2008;29:4862. [PubMed: 19130568]
21. Rubinstein I, Shtilman L. J. Chem. Soc. Faraday T. II 1979;75:231.
22. Rubinstein I, Zaltzman B, Lerman I. Phys. Rev. E 2005;72:011505.
23. Pu Q, Yun J, Temkin H, Liu S. Nano Lett 2004;4:1099.
24. Plecis A, Schoch RB, Renaud P. Nano Lett 2005;5:1147. [PubMed: 15943459]
25. Wang YC, Han J. Lab Chip 2008;8:392. [PubMed: 18305855]
26. Jin X, Joseph S, Gatimu EN, Bohn PW, Aloru NR. Langmuir 2007;23:13209. [PubMed: 17999544]
27. Kim SJ, Wang YC, Lee JH, Jang H, Han J. Phys. Rev. Lett 2007;99:044501. [PubMed: 17678369]
28. Kim SJ, Han J. Anal. Chem 2008;80:3507. [PubMed: 18380489]
29. Mao P, Han J. Lab Chip 2005;5:837. [PubMed: 16027934]
30. Dhopeshwarkar R, Crooks RM, Hlushkou D, Tallarek U. Anal. Chem 2008;80:1039. [PubMed: 18197694]
31. Rubinstein I, Zaltzman B. Phys. Rev. E 2000;62:2238.
32. Ben Y, Chang HC. J. Fluid Mech 2002;461:229.
33. Ben Y, Demekhin EA, Chang HC. J. Colloid Interf. Sci 2004;276:483.
34. Molho JI, Herr AE, Mosier BP, Santiago JG, Kenny KW, Brennen RA, Gordon GB, Mohammadi B. Anal. Chem 2001;73:1350.
35. Sinton D. Microfluid. Nanofluid 2004;1:2.
36. Huang KD, Yang RJ. Microfluid. Nanofluid 2008;5:631.
37. Rubinstein SM, Manukyan G, Staicu A, Rubinstein I, Zaltzman B, Lammertink RGH, Mugele F, Wessling M. Phys. Rev. Lett 2008;101:236101. [PubMed: 19113567]
38. Melin J, Quake SR. Annu. Rev. Biophys. Biomol. Struct 2007;36:213. [PubMed: 17269901]

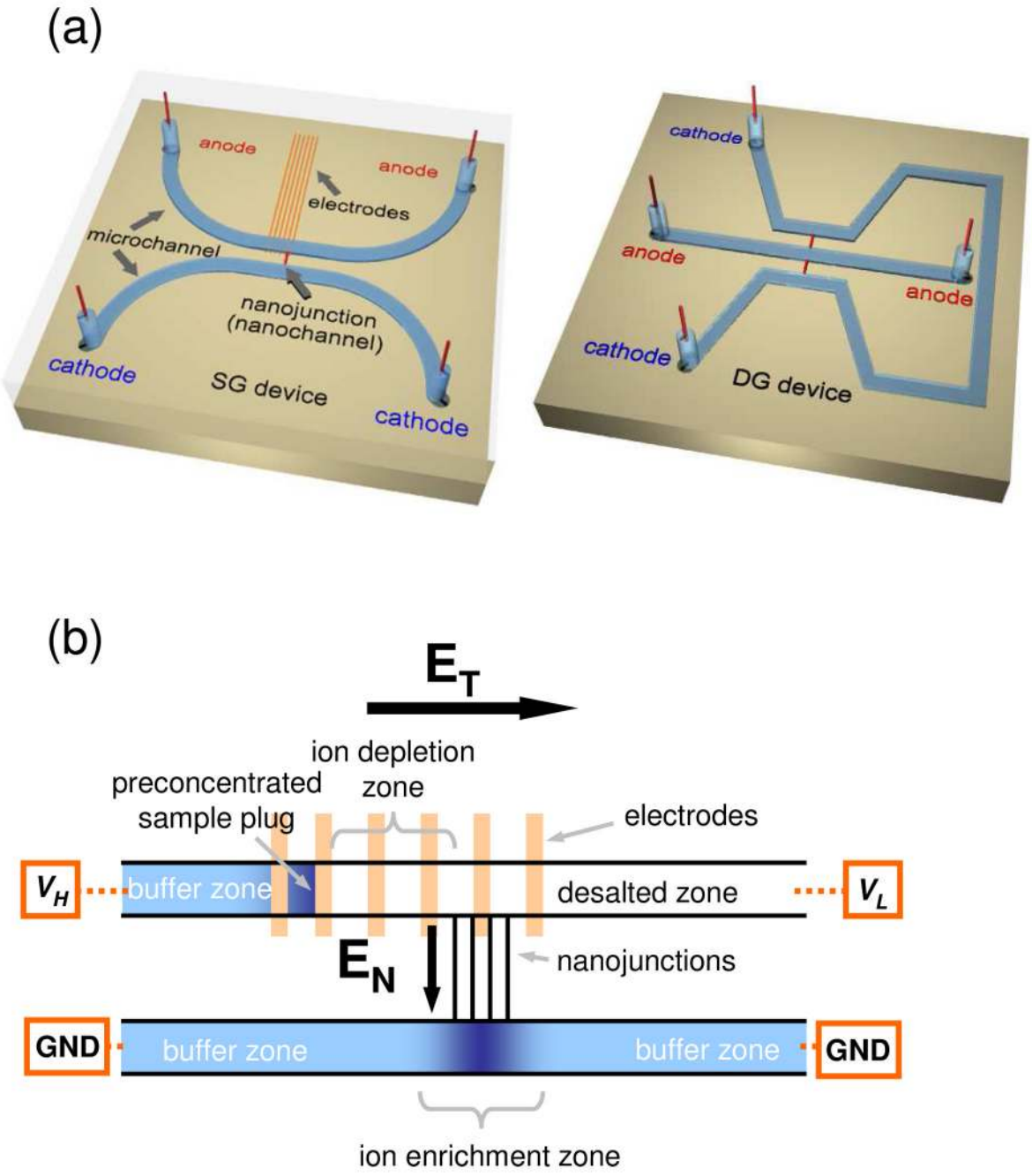

Figure 1.
Schematic diagram of (a) micro/nanofluidic hybrid channel system and (b) electrokinetic configurations under dc bias in the system.

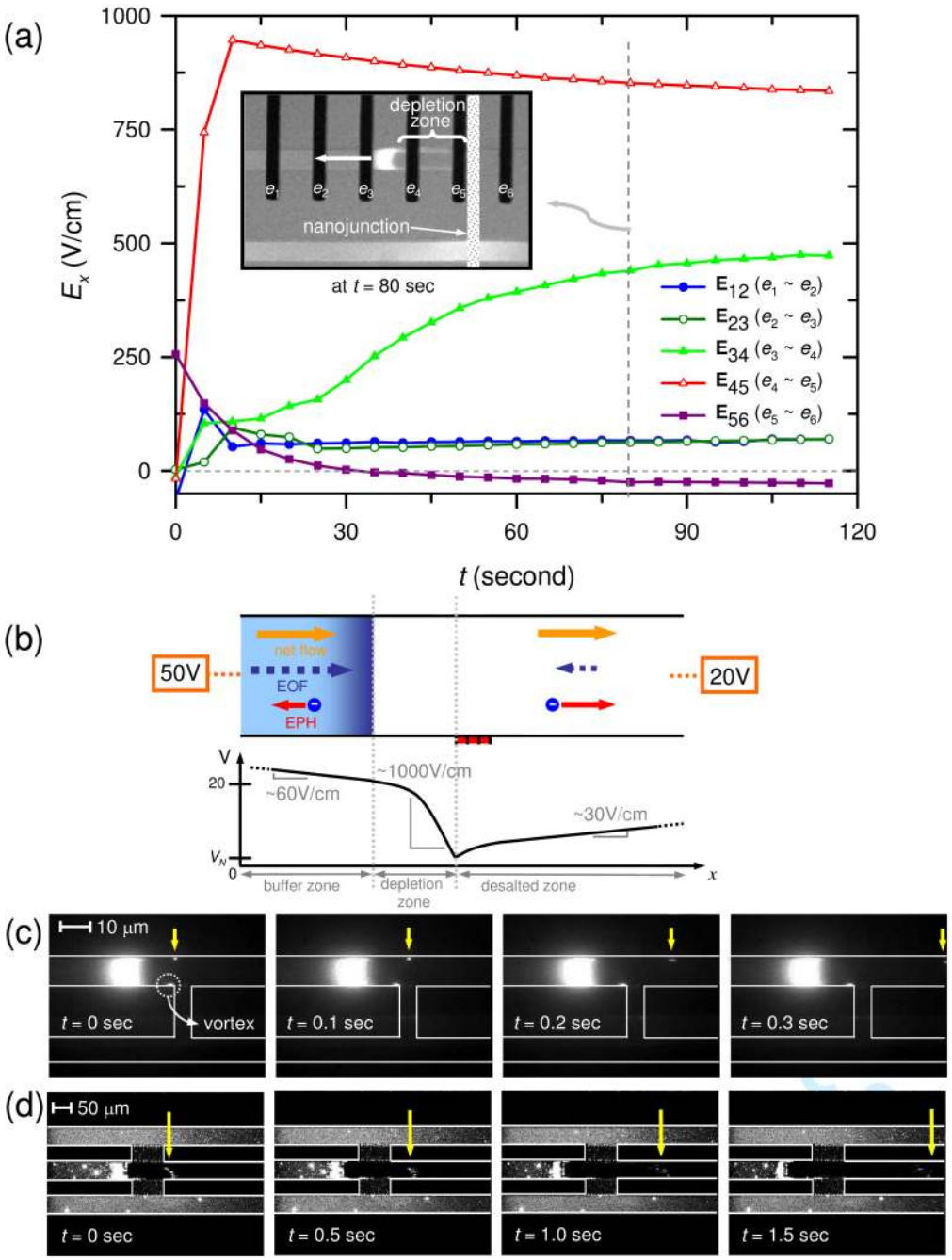

Figure 2.

(a) *In situ* measurement of local electric fields inside and outside the ion depletion using microelectrodes integrated along the microchannel. (b) Schematic plot of electric potential and electrical field along the main microchannel (EPH: electrophoresis).The electrokinetic migration of charged particles in (c) SG and (d) DG device. Estimated velocity of pointed particles was approximately (c) 140μm/sec at V_H = 10V and V_L = 5V and (d) 500μm/sec at V_H = 20V and V_L = 15V.

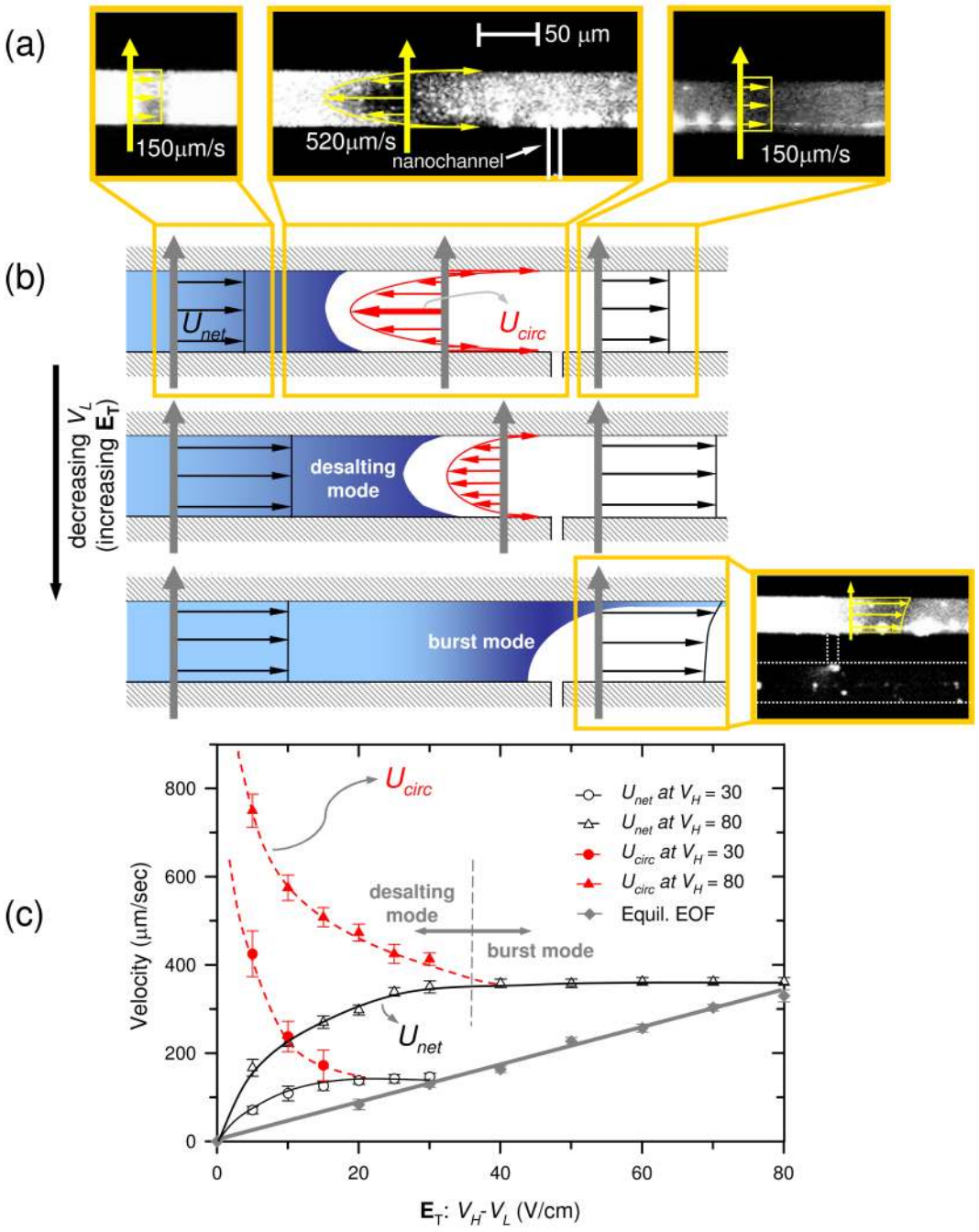

Figure 3.

(a) Details of AEK flow field inside and outside the ion depletion zone by patterened photobleaching technique. (b) Schematics of AEK flow as a function of $\mathbf{E_T}$ and (c) experimental measurement of AEK flow velocity inside and outside the depletion zone.

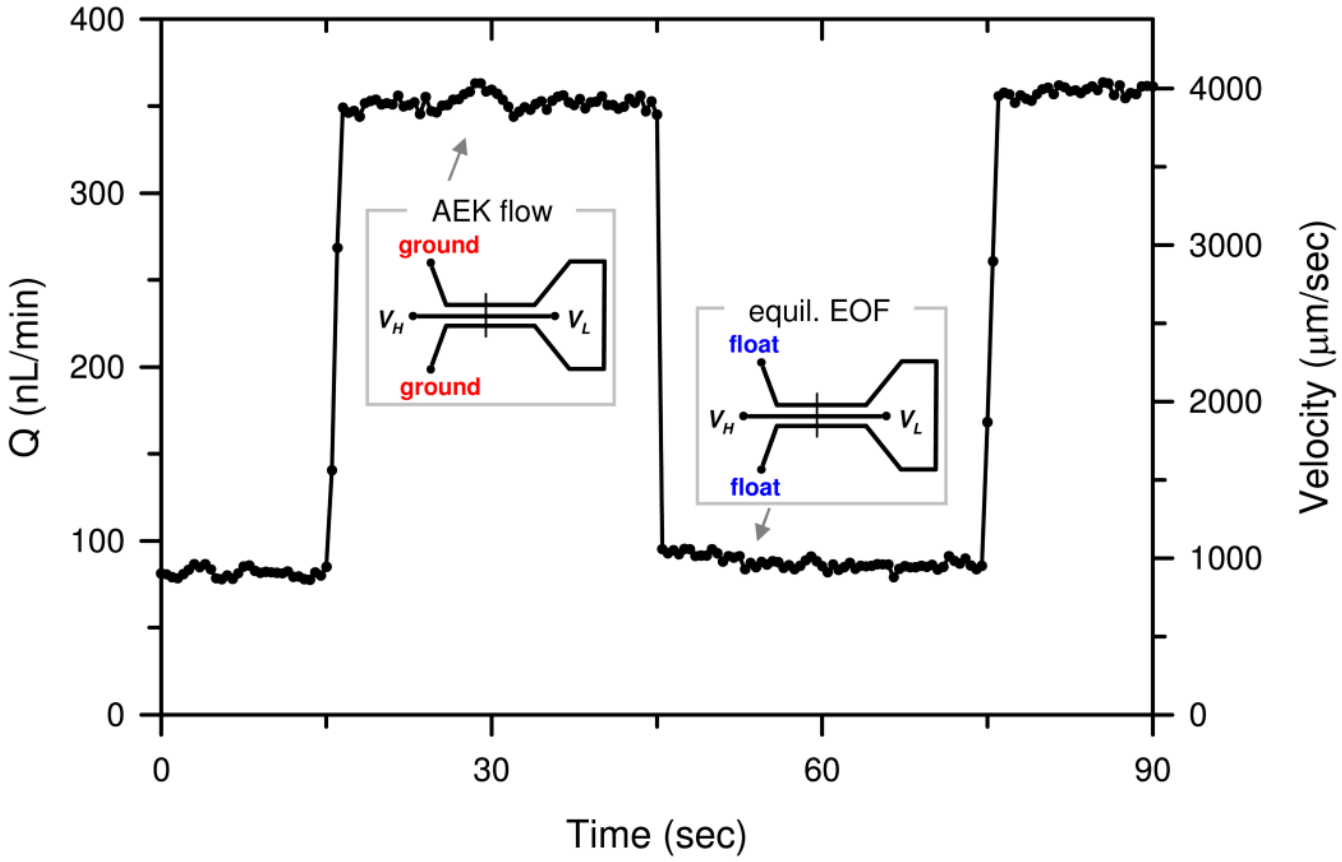

Figure 4.
Fluid pumping using amplified electrokinetic flow (~70nL/min; equil, ~350nL/min; AEK).

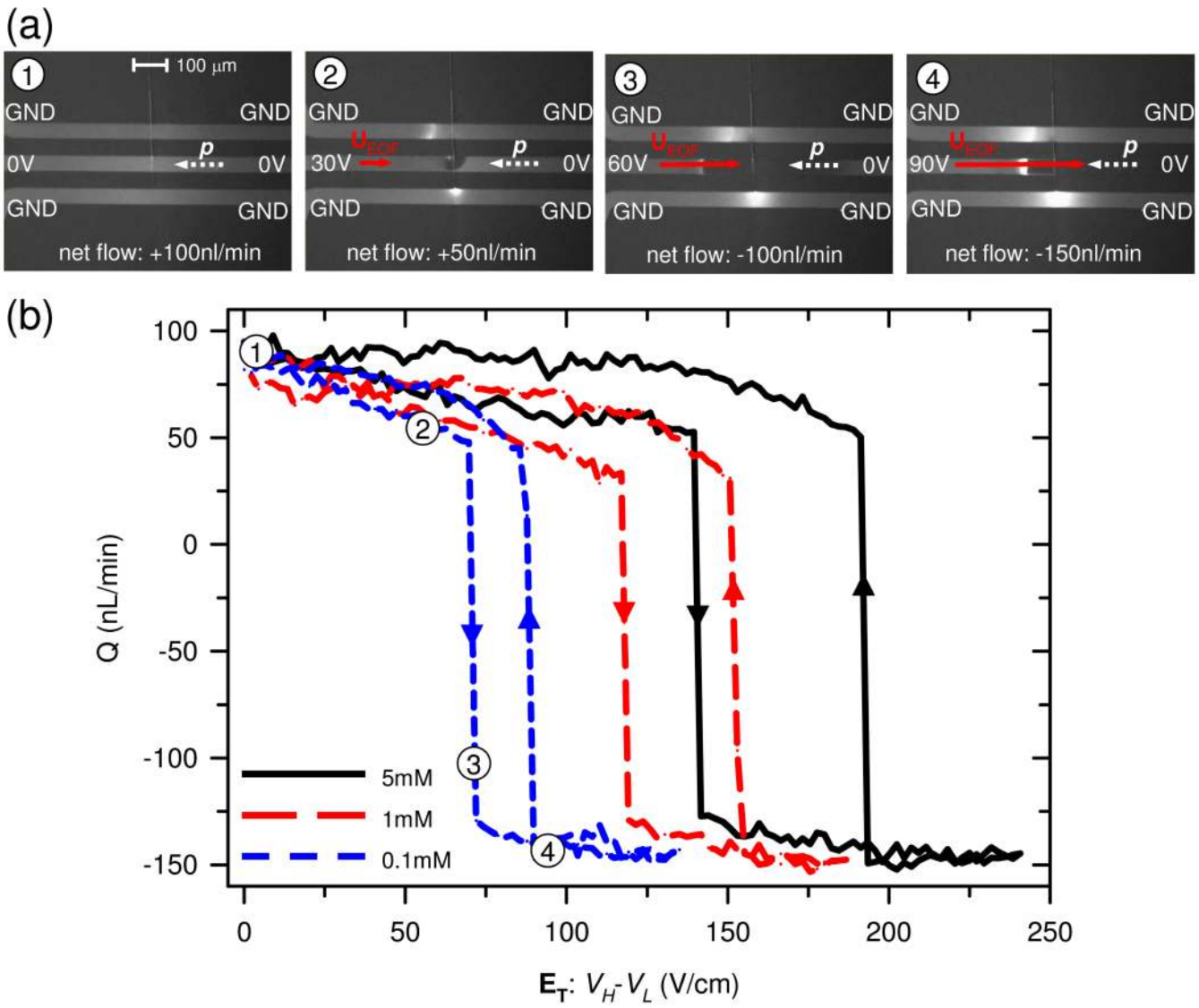

Figure 5.

(a) Sequential images of fluid switching using AEK flow. Right-dotted arrow designated external pressure-driven flow, while the left arrow designate AEK flow which reverses the external pressure-driven flow. (b) Fluid pumping hysteresis as a function of $\mathbf{E_T}$ and buffer ionic concentration.